# Interference Characterization and Power Optimization for Automotive Radar with Directional Antenna

Ping Chu, J. Andrew Zhang, Xiaoxiang Wang, Zesong Fei, Gengfa Fang, Dongyu Wang

***Abstract*—Wide deployment of radar sensors on automotive vehicles can potentially lead to a severe interference problem. Such interference has been characterized without considering directional antenna patterns, which could lead to results significantly larger than the actual ones. In this paper, we study the mean power of effective echo signals and interference, by considering both front- and side- mounted radars equipped with directional antennas. We employ the stochastic geometry method to characterize the randomness of vehicles and hence radars in both two-lane and multi-lane scenarios, and derive closed-form expressions for the mean interference by approximating the radiation pattern by Gaussian waveforms. Simulation results are shown to match the analytical results very well, and insights are obtained for the impact of radar parameters on interference. Based on the interference analysis, we aim to minimize the total transmission power of each vehicle with constraints on the required signal to interference and noise ratio. An optimal solution is obtained based on linear programming techniques and corroborated by simulation results.**

***Index Terms*—Automotive radars, Radar-to-radar interference, Stochastic Geometry, Interference modelling, Power allocation**

## I. Introduction

Automotive radar is becoming an essential configuration in smart transportation systems, such as self-driving cars and advanced driver assistant systems [1], [2]. It plays a key role in detecting and interpreting obstacles for improving driving safety, reducing driver stress and adding life-saving preventative interventions. In the last few years, automotive radar systems have become common on high-end vehicles and are now being installed on more electronic models, too. In the near future, we will see wide deployment and usage of automotive radar on the road.

The increasing usage of automotive radar sensors potentially leads to increasing occurrence of radar-to-radar interference. The reception of unwanted signals from other automotive radar sensors is usually called mutual interference between automotive radar sensors [3]. Such interference happens when they use the same frequency channel and within the range of their respective coverage. The reception of interference signals can lead to problems such as ghost targets or a reduced signal-to-noise power ratio (SNR). In the real road traffic situation, mutual interference between different automotive radars is unavoidable due to the resource reusing. For example, forward- and sideward- looking radars interfere with their peers travelling in the opposition direction or crossroads. Backward-looking radars can interfere the forward- and sideward- looking radars in the same direction.

There have been some studies on radar interference modelling. In [4], the mutual interference between FMCW radars was analysed and the effect of interference on radar performance was evaluated. In [5], interference was investigated for different types of radars under different conditions (e.g., weather condition and vehicular position). Detailed causes to mutual interference for two types of radar sensors were analyzed. In [6], a simulation-based predictor using ray-tracing was proposed for modelling the received power levels for useful echo and interference signals. In [7], a stochastic geometry method was adopted to analyze radar interference, where vehicle locations are assumed to follow two types of point models including a linear Poisson Point Process (PPP) and a fully regular lattice. It is shown that the mean interference is independent of the point models when the width of the road approaches zero.

To mitigate radar interference, techniques such as resource allocation [8], [9] and interference mitigation [10], [11] have been proposed. In [8], a power allocation strategy based on game theory was proposed for distributed multiple radars in a spectrum sharing environment. In [9], a game theoretic approach was introduced for joint beamforming and power allocation in a distributed radar network and a pricing mechanism was proposed to minimize the inter-radar interference. In [10], an adaptive beamforming approach was developed based on MIMO radar to mitigate wireless interference for radar-wireless spectrum sharing systems. In [11], a frequency-hopping random chirp FMCW technique was proposed to reduce mutual interference for FMCW radars. In [12], two power allocation schemes were proposed for distributed multiple-radar systems to meet a predetermined localization threshold. Optimal resource allocation schemes under various constraints are also investigated for coexisting and integrated radar and communications systems in [13]–[16].

One major limitation of these works is that they do not take into consideration the impact of antenna radiation pattern on interference modelling and then mitigation. In [7], a directional

Ping Chu is with Beijing University of Posts and Telecommunications & University of Technology Sydney, Australia (Email: ping.chu@student.uts.edu.au).

J. Andrew Zhang and Gengfa Fang are with the Global Big Data Technology Centre, University of Technology Sydney, Australia (Email: {Andrew.Zhang; gengfa.fang}@uts.edu.au).

Xiaoxiang Wang and Dongyu Wang are with Beijing University of Post and Telecommunication, Beijing, China (Email: {cpwang; dy_wang}@bupt.edu.cn).

Zesong Fei is with the School of Information and Electronics, Beijing Institute of Technology, Beijing 100081, China (E-mail: feizesong@bit.edu.cn).

antenna was considered but it was assumed that the gain in the main-lobe is the same and the side-lobe was disregarded. Using a flat main-lobe may cause exaggerated interference, while ignoring side-lobes leads to under-estimated interference, particularly when each signal for sensing is typically very small and can be comparable to the interference received through the side-lobes [5], [17]. Nevertheless, stochastic geometry is a powerful tool for characterizing the randomness of vehicles' locations [7], [18], [19]. It has been widely used for modelling nodes in cellular networks [20], femtocells [21], and vehicular networks [22], [23]. It is particularly useful for vehicular networks where both transmitters and receivers are randomly located and moving. Random geometric graph [24] is also a useful tool for performance analysis and optimization of large wireless networks. Compared with random geometric graphs, stochastic geometry enables more flexible and tailored analysis, e.g., studying the average behavior over many spatial realizations of a network, where nodes are placed according to specified probability distribution.

In this paper, applying the stochastic geometry model, we develop a signal and interference power analysis framework for automotive radars, by considering both front-mounted (FR) and side-mounted radars (SR), and directional antenna radiation patterns. We first study a two-lane scenario and then extend the work to a multi-lane one. Using the stochastic geometry model to formulate the vehicular location distribution in a road segment, we derive the expressions for the mean power of effective echo signals and the interference, taking into consideration of frequency reuse factor, vehicle density, and radiation patterns for FR and SR. Assuming a Gaussian waveform for the antenna radiation pattern, we provide closed-form expressions for their mean interference power. We then investigate how to minimize the total transmission power while guaranteeing an average signal-to-interference-and-noise ratio (SINR) for radar sensing. Extensive simulation results are provided and found to match analytical results very well.

The major contributions of this work are listed as follows:

- We propose an analytic framework for evaluating the mean interference experiencing by autonomous radars with directional antennas in both two-lane and multi-lane scenarios, based on the stochastic geometry method. This framework enables the incorporation of any antenna radiation pattern into the analysis.
- We provide closed-form expressions for the mean interference power by approximating the antenna radiation pattern with a Gaussian function. This approximation is shown to be accurate for uniform linear arrays (ULA) according to simulation results. The closed-form expressions provide important insights on the dependence of interference on system parameters.
- We provide a closed-form solution to the problem of minimizing the total transmission power of FR and SR, when the desired minimum SINRs for FR and SR are subject to given thresholds. The optimization results are corroborated by simulation results.

The remainder of this paper is organized as follows. Section II introduces the system and stochastic geometric model, and formulates the echo and interference signals. In Section III, considering a two-lane scenario, we present the analytical framework for mean interference characterization, and present closed-form expressions with Gaussian approximation. Section IV extends the results to a multi-lane scenario. In Section V, we present the power minimization algorithm. Finally, simulation results are provided in Section VI, and Section VII concludes the paper.

Notations: $\overline{x}$ denotes the mean of $x$. Random variables are denoted in bold. $\mathbb{E}[\mathbf{x}]$ denotes the expectation of $\mathbf{x}$. $\|\mathbf{x}\|$ denotes the norm of the vector $\mathbf{x}$.

## II. System and Signal Models

In this section, we adopt stochastic geometry methods to construct the system model and emulate geometric distribution of vehicles on a two-lane road and the radio propagation of associated radars. Without loss of generality, we consider a vehicle located at the origin of one lane and call it the *typical vehicle*, and assume that its statistical behaviour is typical and representative of all other vehicles. We consider a temporal snapshot of the road traffic during which the vehicles can be considered as stationary, preserving the geometric statistics of the traffic. We note that these statistics are indeed not constant over a long period. However, they are of a slow kinetic nature and can be safely regarded as static for a given segment of a road over a reasonable observation period.

### A. Geometrical Model

Automotive radar is used to locate objects in the vicinity of the hosting vehicle. A modern vehicle could be equipped with more than one radar. Automotive radars can be categorized into three types based on detection capabilities: long range radar (LRR) which is used for measuring the relative speed and distance of other vehicles, medium range radar (MRR) which is used for detecting objects in a wider field of view (e.g., for cross traffic alert systems), and short range radar (SRR) which is used for sensing in the vicinity of the car (e.g., for parking aid or obstacle detection). The LRR, as well as MRR, are mounted on the front of the vehicle, and SRR, as well as MRR, are mounted on the sides and back of the vehicle. Different field of views (FoVs) are demanded for these three types of automotive radars.

In this paper, we consider the setup where a vehicle is equipped with one FR for adaptive cruise control and two SRs for side impact. Generally, automotive radars are equipped with directional antennas which generate directional beams with main and side lobes. The beamwidth of different radars is generally different. Assume that all vehicles are equipped with the same types of FR and SR.

We consider a two-way road with one lane in each direction. Assume that the lanes are of equal width of $L$, and vehicle travel in the middle of the lane. We assume that there is no coordination between the frequency band that a radar uses. A radar just randomly selects its frequency band. When radars use the same frequency band, interference can be potentially generated. Fig. 1 illustrates a simplified layout of the interfering FR/SR radars. Only the beam from one SR is

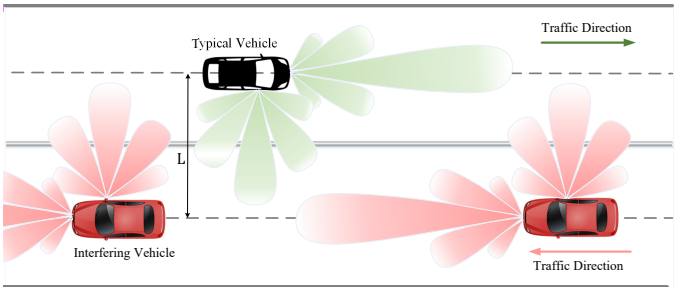


Fig. 1. The interference between automotive radars. (Red vehicles stand the interfering ones.)

plotted for each vehicle, as the other one causes negligible interference to other radars in the setup. We assume that the interference to a FR and SR is mainly from the FR and SR of vehicles travelling in the opposite direction.

We capture the randomness of vehicle location using the popular geometrical distribution of PPP. In each lane, the locations of vehicles follow a unidimensional PPP [25] in $\mathbb{R}^1$ with a homogeneous linear density $\rho$ measured in vehicles per unit length. We denote the set of vehicles in one lane as $\Phi_{\text{PPP}}$. Let $\xi$ denote the probability that a vehicle in the opposing lane uses the same frequency with the typical vehicle. Considering the interference from other vehicles to the typical one, we can describe the interferers by applying a random marking as

$$\Theta_{\text{PPP}} = \{i : i \in \Phi_{\text{PPP}}, \mathcal{M}(i) = 1\}, \tag{1}$$

where the mark $\mathcal{M}(i)$ is defined for different interfering scenarios as follows:

- From FR to FR or from FR to SR,

$$\mathcal{M}(i) = \begin{cases} 0, & \ell_i \le 0, \\ \boldsymbol{B}(\xi), & \ell_i > 0, \end{cases} \tag{2}$$

  where $\ell_i$ denotes the location of vehicle $i$, the interference between FR and FR is zero for $\ell \le 0$, and $\boldsymbol{B}(\xi)$ is a Bernoulli random variable with selection probability $\xi$; and
- Between SR and SR,

$$\mathcal{M}(i) = \boldsymbol{B}(\xi), \ i \in \Phi_{\text{PPP}}. \tag{3}$$

### B. Radar Reception

Each radar may receive two types of impacting signals including *radar echo signal* and *interference signals*. The echo signal is transmitted by the typical vehicle and the reflected signal is used for object localization. The interference signals are from other radars using the same frequency band with the typical vehicle. For interference signals, we use the inverse square law of the distance for signal attenuation analysis. For the effective power of echo signals, we only take into consideration of directly reflected paths from targets. For interference analysis, we consider an additional gain factor corresponding to a statistical fading process, to account for multipath propagations.

In this paper, we only consider signals coming from the horizontal plane, and hence a two-dimension model is adopted for signal and interference analysis. The ideas presented in this paper can be extended to three-dimension models.

We assume effective echo signals are coming from the direction corresponding to the maximum antenna gain, and hence the results serve as upper bounds for other target directions.

*1) Radar Echo-Signal:* The power of received echo-signal is well characterized, for example, in [26]. For FR, it can be represented as

$$\begin{aligned} S_r^f &= \frac{P_f G_f}{4\pi R_f^{-2}} \times \frac{\sigma_c^f}{4\pi R_f^{-2}} A_e^f \\ &= \underbrace{\underbrace{\frac{P_f G_f}{4\pi R_f^{-2}}}_{\text{Incident power density}} \times \frac{\sigma_c^f}{4\pi R_f^{-2}}}_{\text{Reflected power density}} \times \underbrace{\frac{G_f \lambda_f^2}{4\pi}}_{\text{Effective area of receiving antenna}} \\ &= \varepsilon_1^f \varepsilon_2^f \varepsilon_3^f P_f R_f^{-4}, \end{aligned} \tag{4}$$

where $P_f$ is the FR transmission power, $R$ is the distance between radar and target, $G_f$ and $A_e^f$ are the maximum antenna gain and the effective area of receiving antenna, respectively, and $\sigma_c^f$ is the cross-section area (RCS) of the target. The parameters $\varepsilon_1^f$, $\varepsilon_2^f$ and $\varepsilon_3^f$ are given by

$$\varepsilon_1^f = \frac{G_f}{4\pi}, \varepsilon_2^f = \frac{\sigma_c^f}{4\pi} \text{ and } \varepsilon_3^f = \frac{G_f \lambda_f^2}{4\pi} = \frac{G_f}{4\pi}\left(\frac{c}{f_f}\right)^2, \tag{5}$$

where $f_f$ is the central operating frequency and $c$ is the speed of light.

Similarly, the received power of echo-signal for SR can be written as

$$S_r^s = \frac{P_s G_s}{4\pi R_s^{-2}} \times \frac{\sigma_c^s}{4\pi R_s^{-2}} A_e^s = \varepsilon_1^s \varepsilon_2^s \varepsilon_3^s P_s {R_s}^{-4}, \tag{6}$$

where $P_s$ is the SR transmission power, and

$$\varepsilon_1^s = \frac{G_s}{4\pi}, \varepsilon_2^s = \frac{\sigma_c^s}{4\pi} \text{ and } \varepsilon_3^s = \frac{G_s {\lambda_s}^2}{4\pi} = \frac{G_s}{4\pi}\left(\frac{c}{f_s}\right)^2. \tag{7}$$

Symbols with subscript $s$ are defined for SR accordingly.

*2) Interference Signals:* We introduce a random vector $\mathbf{H}_i$, where $i$ refers to the $i$-th interfering vehicle, to account for the statistical channel fading for interfering signals. This randomness is caused by multipath propagation due to reflections from buildings, vegetation, and other vehicles. We assume that the elements of this random vector are identically and independently distributed (i.i.d.), because of the homogeneous fading environment.

The interference signals from FR and SR of vehicle $i$ to the FR of the typical one can be expressed by

$$\begin{aligned} I_i^f &= I_i^{ff} + I_i^{sf} \\ &= \Big( \underbrace{\varepsilon_1^f \ P_f \ g^f(\beta_i)}_{\text{(a) FR Interference power.}} + \underbrace{\varepsilon_1^s \ P_s \ g^s(\pi/2 - \beta_i)}_{\text{(b) SR Interference power.}} \Big) \cdot \\ &\quad \underbrace{\varepsilon_3^f \ g^f(\beta_i)}_{\text{(c) Rx antenna gain of FR.}} \quad \mathbf{H}_i \|r_i\|^{-2} \end{aligned} \tag{8}$$

where $I_i^{ff}$ and $I_i^{sf}$ denote the interference from FR and SR to FR, respectively, $\|r_i\|$ is the distance between the typical

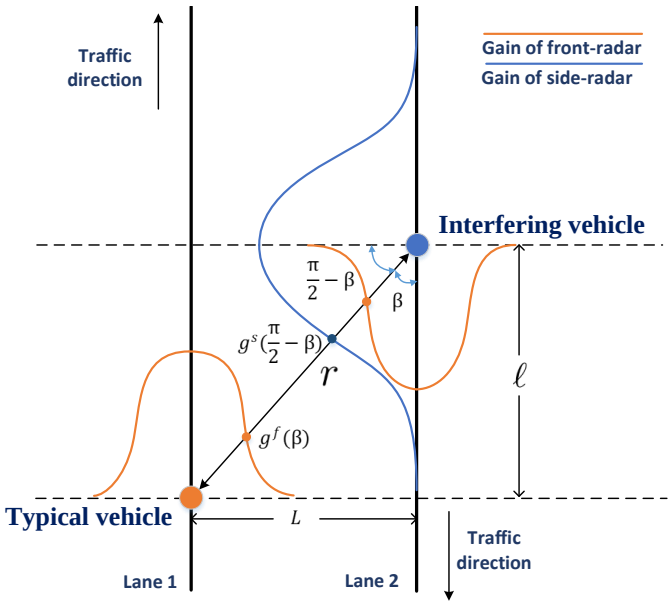


Fig. 2. Illustration of the signal strength and interference between automotive radars in different directions.

and interfering vehicles, $\beta_i$ is the angle between the moving direction and the line connecting the two vehicles, $g^f(\beta_i)$ and $g^s(\beta_i)$ denote the normalized antenna radiation pattern (or antenna gain) as a function of signal incoming direction $\beta$, with a maximum of 1, for FR and SR, respectively. As shown in Fig. 2, $\beta_i$ can be expressed as $\beta_i = \arcsin(L/r_i)$. In (8), part (a) and (b) denote the power of interference signals transmitted in the direction of $\beta_i$ from FR and SR, respectively, and part (c) denotes the receiver antenna gain in the direction of $\beta_i$.

Similarly, we can represent the interference to SR as

$$\begin{aligned} I_i^s &= I_i^{fs} + I_i^{ss} \\ &= ( \underbrace{\varepsilon_1^f P_f \; g^f(\beta_i)}_{\text{(a) FR Interference power.}} + \underbrace{\varepsilon_1^s P_s \; g^s(\pi/2-\beta_i)}_{\text{(b) SR Interference power.}} ) \\ &\quad \underbrace{\varepsilon_3^s \; g^s(\pi/2-\beta_i)}_{\text{(c) Rx antenna gain of SR.}} \; \mathbf{H}_i \|r_i\|^{-2}. \end{aligned} \tag{9}$$

## III. Interference Characterization in Two-Lane Scenarios

In this section, we first derive general expressions for mean interference power in order to get a general sense on main parameters that affect the interference value and then derive closed-form expressions by using a specific Gaussian waveform to approximate the antenna radiation pattern. The results here are also applicable to vehicles in the most left and right lanes in a multi-lane scenario.

### A. General Expressions

Assume that the interference signals from vehicles are statistically independent. The total interference power received at the typical vehicle can be written as

$$\begin{aligned} \boldsymbol{I}^f &= \sum_{i\in\Theta_{\text{PPP}}} I_i^f \\ &= \sum_{i\in\Theta_{\text{PPP}}} \Big[ \big(\varepsilon_1^f P_f g^f(\beta_i) + \varepsilon_1^s P_s g^s(\pi/2-\beta_i)\big) \cdot \\ &\quad \varepsilon_3^f g^f(\beta_i) \mathbf{H}_i \|r_i\|^{-2} \Big], \text{ and} \end{aligned} \tag{10}$$

$$\begin{aligned} \boldsymbol{I}^s &= \sum_{i\in\Theta_{\text{PPP}}} I_i^s \\ &= \sum_{i\in\Theta_{\text{PPP}}} \Big[ \big(\varepsilon_1^f P_f g^f(\beta_i) + \varepsilon_1^s P_s g^s(\pi/2-\beta_i)\big) \cdot \\ &\quad \varepsilon_3^s g^s(\pi/2-\beta_i) \mathbf{H}_i \|r_i\|^{-2} \Big], \end{aligned} \tag{11}$$

for FR and SR, respectively, where $\Theta_{\text{PPP}}$ denotes the set of interfering vehicles characterized by PPP.

According to the Campbell theorem [27] [page 281], we can calculate the statistical mean of the interference power at FR as follows

$$\begin{aligned} \overline{I^f} &= \mathbb{E}\left[\boldsymbol{I}^f\right] = \overline{I^{ff}} + \overline{I^{sf}} \\ &= \underbrace{\mathbb{E}_H\left[\mathbb{E}_{\Theta_{\text{PPP}}}\left[\sum_{i\in\Theta_{\text{PPP}}} \varepsilon_1^f P_f g^f(\beta_i) \varepsilon_3^f g^f(\beta_i) \|r_i\|^{-2}\right]\right]}_{\text{Mean interference from FR to FR}} + \\ &\quad \underbrace{\mathbb{E}_H\left[\mathbb{E}_{\Theta_{\text{PPP}}}\left[\sum_{i\in\Theta_{\text{PPP}}} \varepsilon_1^s P_s g^s\left(\frac{\pi}{2}-\beta_i\right) \varepsilon_3^f g^f(\beta_i) \|r_i\|^{-2}\right]\right]}_{\text{Mean interference from SR to FR}} \\ &\overset{\text{e}}{=} \mathbb{E}_H[H] \left\{ \rho_I \varepsilon_1^f \varepsilon_3^f P_f \int_0^{+\infty} \left[g^f\left(\arcsin\frac{L}{r(\ell)}\right)\right]^2 r(\ell)^{-2} d\ell + \right. \\ &\quad \left. \rho_I \varepsilon_1^s \varepsilon_3^f P_s \int_0^{+\infty} g^s(\frac{\pi}{2} - \arcsin\frac{L}{r(\ell)}) g^f(\arcsin\frac{L}{r(\ell)}) r(\ell)^{-2} d\ell \right\} \\ &= \rho_I \left\{ \varepsilon_1^f \varepsilon_3^f P_f \int_0^{+\infty} \left[g^f(\arcsin\frac{L}{r(\ell)})\right]^2 r(\ell)^{-2} d\ell + \right. \\ &\quad \left. \varepsilon_1^s \varepsilon_3^f P_s \int_0^{+\infty} g^s(\frac{\pi}{2} - \arcsin\frac{L}{r(\ell)}) g^f(\arcsin\frac{L}{r(\ell)}) r(\ell)^{-2} d\ell \right\}. \end{aligned} \tag{12}$$

In (12), $\mathbb{E}_H[\cdot]$ denotes the expectation over the statistical fading channel, $\mathbb{E}_{\Theta_{\text{PPP}}}$ is the expectation over all interfering vehicles with numbers and their locations following PPP, $\rho_I$ is the density of interfering vehicles measured in [cars/unit length] and $\rho_I = \xi\rho$, and $r(\ell) = \sqrt{(L^2+\ell^2)}$. The step (e) follows the assumption that individual propagation channels are i.i.d, and are uncorrelated to the geometrical point process. The final step uses the assumption that the average channel gain is normalized to the unity i.e., $\mathbb{E}_H[H] \triangleq u_H = 1$.

Similarly, we can obtain the mean power of the interference at SR and present it in (13), as shown at the top of next page.

From (12) and (13), we can have the following observations:

- The mean interference from FR and SR of interfering vehicles are linearly and monotonically increasing function

$$\begin{aligned}\overline{I^s} &= \overline{I^{fs}} + \overline{I^{ss}} \\ &= \underbrace{\mathbb{E}_H\left[\mathbb{E}_{\Theta_{\text{PPP}}}\left[\sum_{i\in\Theta_{\text{PPP}}} \varepsilon_1^f P_f g^f(\beta_i)\varepsilon_3^s g^s\left(\frac{\pi}{2}-\beta_i\right)\|r_i\|^{-2}\right]\right]}_{\text{Mean Interference from FR to SR}} + \underbrace{\mathbb{E}_H\left[\mathbb{E}_{\Theta_{\text{PPP}}}\left[\sum_{i\in\Theta_{\text{PPP}}} \varepsilon_1^s P_s g^s\left(\frac{\pi}{2}-\beta_i\right)\varepsilon_3^s g^s(\frac{\pi}{2}-\beta_i)\|r_i\|^{-2}\right]\right]}_{\text{Mean Interference from SR to SR}} \\ &= \rho_I\left\{\varepsilon_1^f\varepsilon_3^s P_f\int_0^{+\infty} g^f(\arcsin\frac{L}{r(\ell)})g^s(\frac{\pi}{2}-\arcsin\frac{L}{r(\ell)})r(\ell)^{-2}d\ell + 2\varepsilon_1^s\varepsilon_3^s P_s\int_0^{+\infty}\left[g^s(\frac{\pi}{2}-\arcsin\frac{L}{r(\ell)})\right]^2 r(\ell)^{-2}d\ell\right\}.\end{aligned} \tag{13}$$

of their transmission power, respectively. But the total interference to each of FR and SR is a weighted sum of their transmission power and hence is not a linear function of it any more;

- The interference power is linearly proportional to the effective density of the interfering vehicles $\rho_I$, as expected.

In the next section, we consider two special functions for $g^f$ and $g^s$ to get compact results, which provide more insights on the interference.

### *B. Interference with Gaussian Directional Radiation Pattern*

Here, we consider a special example for the antenna radiation pattern ($g^f(\cdot)$ and $g^s(\cdot)$), which can be represented by a normalized Gaussian function. There are two reasons for considering a beam pattern of Gaussian function: (1) It can lead to compact and closed-form expressions; and (2) it provides a good approximation to actual beam patterns as will be shown in Section VI. The gain function $g^f(\beta)$ and $g^s(\beta)$ are given by

$$\begin{cases} g^f(\beta) = \exp(-\dfrac{\beta^2}{2\sigma_f^2}), \beta\in[-\dfrac{\pi}{2},\dfrac{\pi}{2}], \\ g^s(\beta) = \exp(-\dfrac{\beta^2}{2\sigma_s^2}), \beta\in[-\dfrac{\pi}{2},\dfrac{\pi}{2}], \end{cases} \tag{14}$$

where $\sigma_f^2$ and $\sigma_s^2$ are the parameters of the Gaussian function and are adjustable. From Fig. 2, we have $\ell = L/\tan(\beta)$. For the directional antenna, applying (14) to (12) and (13), we can obtain

$$\begin{aligned}\overline{I^f} &= \overline{I^{ff}} + \overline{I^{sf}} \\ &= \frac{\rho_I\varepsilon_1^f\varepsilon_3^f P_f}{L}\int_0^{\frac{\pi}{2}}\exp\left(-\frac{\beta^2}{\sigma_f^2}\right)d\beta + \\ &\frac{\rho_I\varepsilon_1^s\varepsilon_3^f P_s}{L}\int_0^{\frac{\pi}{2}}\exp\left(-\frac{\left(\frac{\pi}{2}-\beta\right)^2}{2\sigma_s^2}-\frac{\beta^2}{2\sigma_f^2}\right)d\beta \\ &= \frac{\sqrt{\pi}}{2L}\xi\rho\left(u_{\sigma_f}\varepsilon_1^f\varepsilon_3^f P_f + u_{\sigma_{f,s}}\varepsilon_1^s\varepsilon_3^f P_s\right),\end{aligned} \tag{15}$$

and

$$\begin{aligned}\overline{I^s} &= \overline{I^{fs}} + \overline{I^{ss}} \\ &= \frac{\rho_I\varepsilon_1^f\varepsilon_3^s P_f}{L}\int_0^{\frac{\pi}{2}}\exp\left(-\frac{\beta^2}{2\sigma_f^2}-\frac{\left(\frac{\pi}{2}-\beta\right)^2}{2\sigma_s^2}\right)d\beta + \\ &\frac{2\rho_I\varepsilon_1^s\varepsilon_3^s P_s}{L}\int_0^{\frac{\pi}{2}}\exp\left(-\frac{\left(\frac{\pi}{2}-\beta\right)^2}{\sigma_s^2}\right)d\beta \\ &= \frac{\sqrt{\pi}}{2L}\xi\rho\left(u_{\sigma_{f,s}}\varepsilon_1^f\varepsilon_3^s P_f + 2u_{\sigma_s}\varepsilon_1^s\varepsilon_3^s P_s\right),\end{aligned} \tag{16}$$

where $\text{erf}(x)$ is the Gaussian error function, and

$$\begin{cases} u_{\sigma_f} \triangleq \sigma_f\,\text{erf}(\dfrac{\pi}{2\sigma_f}), \\ u_{\sigma_s} \triangleq \sigma_s\,\text{erf}(\dfrac{\pi}{2\sigma_s}), \\ u_{\sigma_{f,s}} \triangleq \exp\left(-\dfrac{\pi^2}{8\left(\sigma_f^2+\sigma_s^2\right)}\right)\left[\text{erf}\left(\dfrac{\pi\sigma_f}{2\sqrt{2}\sigma_s\sqrt{\sigma_f^2+\sigma_s^2}}\right)\right. \\ \qquad\left. + \text{erf}\left(\dfrac{\pi\sigma_s}{2\sqrt{2}\sigma_f\sqrt{\sigma_f^2+\sigma_s^2}}\right)\right]\dfrac{\sqrt{2}\sigma_f\sigma_s}{\sqrt{\sigma_f^2+\sigma_s^2}}. \end{cases} \tag{17}$$

From (15) and (16), we can get the following observations in addition to those obtained from (12) and (13):

- The mean interference power is linearly proportional to both the frequency reuse factor $\xi$ and the effective density of interfering vehicles $\xi\rho$;
- It is interesting to see that, when the same radar and transmission power is used for FR and SR, $\overline{I^{sf}}$ and $\overline{I^{fs}}$ are largely the same;
- When FR and SR are the same, we can get $\overline{I^{sf}} = \overline{I^{fs}}$ and $\overline{I^{ss}} = 2\overline{I^{ff}}$, and the ratio of total interference between FR and SR is $2/3$. This is because SR and FR see interference from 0 to 180 degrees and 0 to 90 degrees, respectively. Note that this only applies to the two-lane case.

## IV. Extension to Multiple-Lane Scenarios

In this section, we extend the analysis to multiple lanes, as shown in Fig. 3, where there are $m$ lanes in the same direction and $n$ lanes in the opposite direction. We assume that the vehicles in the lanes of each direction follow independent PPP

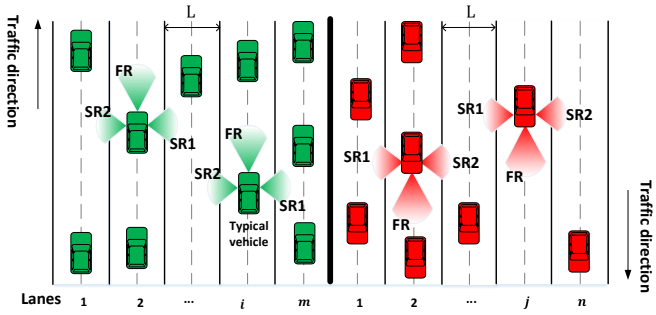


Fig. 3. Illustration of the interference in multiple lanes.

geometrical distribution with density $\rho_i$ and $\rho_j$, ($i \in 1, ..., m$ and $j \in 1, ..., n$), respectively. Assume that the typical vehicle is at a non-edge lane $i$. Referring to Fig. 3, the radar interfering scenarios can be described as follows:

1) *Interference to FR from SRs and FRs:* The interfering SRs include the SR1s on vehicles from the lanes $1, ..., i-1$ and $1, ..., n$, and the SR2s on vehicles from the lanes $i+1, .., m$. The interfering FRs are on vehicles from the lanes $1, ..., n$;
2) *Interference to SR1 from SRs and FRs:* The interfering SRs include the SR2s on vehicles from the lanes $i+1, ..., m$ and the SR1s from the lanes $1, ..., n$. The interfering FRs are on vehicles from the lanes $i+1, ..., m$ and $1, ..., n$;
3) Interference to SR2 from SR1s and FRs on vehicles in the lanes $1, ..., i-1$.

### A. Mean Interference to FR

The mean interference received at the FR on the typical vehicle is given by

$$\overline{I^f} = \overline{I^{ff}} + \overline{I^{s_1 f}} + \overline{I^{s_2 f}}, \tag{18}$$

where $\overline{I^{s_1 f}}$ and $\overline{I^{s_2 f}}$ denote the mean interference from SR1 and SR2 to the FR, respectively. Similar to the analytical method in Section III, we can get the following results with the Gaussian radiation pattern function:

$$\overline{I^{ff}} = \frac{\sqrt{\pi}}{2L} \sum_{j=1}^{n} \frac{1}{m-i+j} u_{\sigma_f} \xi_j \rho_j \varepsilon_1^f \varepsilon_3^f P_f, \tag{19}$$

$$\overline{I^{s_1 f}} = \frac{\sqrt{\pi}}{2L} \left[ \sum_{j=1}^{n} \frac{\xi_j \rho_j}{m-i+j} + \sum_{k=1}^{i-1} \frac{\xi_k \rho_k}{i-k} \right] u_{\sigma_{f,s}} \varepsilon_1^s \varepsilon_3^f P_{s_1}, \tag{20}$$

and

$$\overline{I^{s_2 f}} = \frac{\sqrt{\pi}}{2L} \sum_{k=i+1}^{m} \frac{\xi_k \rho_k}{k-i} u_{\sigma_{f,s}} \varepsilon_1^s \varepsilon_3^f P_{s_2}, \tag{21}$$

where $P_{s_1}$ and $P_{s_2}$ denote the transmission power of SR1 and SR2, respectively, and $\xi_k$ and $\xi_j$ represent the frequency reusing probabilities.

### B. Mean Interference to SR1

The mean interference to SR1 is given by

$$\overline{I^{s_1}} = \overline{I^{f s_1}} + \overline{I^{s_2 s_1}} + \overline{I^{s_1 s_1}}, \tag{22}$$

where $\overline{I^{f s_1}}$, $\overline{I^{s_2 s_1}}$ and $\overline{I^{s_1 s_1}}$ denote the mean interference power from FR to SR1, from SR2 to SR1, and from SR1 to SR1, respectively.

Referring to Section III, we can derive the following results,

$$\overline{I^{f s_1}} = \frac{\sqrt{\pi}}{2L} \left[ \sum_{k=i+1}^{m} \frac{\xi_k \rho_k}{k-i} + \sum_{j=1}^{n} \frac{\xi_j \rho_j}{m-i+j} \right] u_{\sigma_{f,s}} \varepsilon_1^f \varepsilon_3^s P_f, \tag{23}$$

$$\overline{I^{s_2 s_1}} = \frac{\sqrt{\pi}}{L} \sum_{k=i+1}^{m} \frac{\xi_k \rho_k}{k-i} u_{\sigma_s} \varepsilon_1^s \varepsilon_3^s P_{s_2}, \tag{24}$$

and

$$\overline{I^{s_1 s_1}} = \frac{\sqrt{\pi}}{L} \sum_{j=1}^{n} \frac{\xi_j \rho_j}{m-i+j} u_{\sigma_s} \varepsilon_1^s \varepsilon_3^s P_{s_1}. \tag{25}$$

### C. Mean Interference to SR2

The mean interference to SR2 is given by

$$\overline{I^{s_2}} = \overline{I^{f s_2}} + \overline{I^{s_1 s_2}}, \tag{26}$$

where $\overline{I^{f s_2}}$ and $\overline{I^{s_1 s_2}}$ denote the mean interference power from FR to SR2 and from SR1 to the SR2, respectively. We can obtain the following results,

$$\overline{I^{f s_2}} = \frac{\sqrt{\pi}}{2L} \sum_{k=i}^{i-1} \frac{\xi_k \rho_k}{i-k} u_{\sigma_{f,s}} \varepsilon_1^f \varepsilon_3^s P_f, \tag{27}$$

and

$$\overline{I^{s_1 s_2}} = \frac{\sqrt{\pi}}{L} \sum_{k=1}^{i-1} \frac{\xi_k \rho_k}{i-k} u_{\sigma_s} \varepsilon_1^s \varepsilon_3^s P_{s_1}. \tag{28}$$

## V. Minimization of Radar Transmission Power

The SINR is an important parameter that determines the detection performance of vehicular radar. In this section, we study how to minimize the total radar transmission power of the typical vehicle when some low thresholds of the mean SINR are to be met. We start with the two-lane scenario and then extend it to multiple lanes.

### A. Optimization in Two-lane Scenarios

The mean SINRs for FR and SR can be represented as

$$\begin{cases} \overline{\gamma_f} = \dfrac{S_r^f}{\overline{I^f} + \sigma_{\eta_f}^2}, & \text{(29a)} \\ \overline{\gamma_s} = \dfrac{S_r^s}{\overline{I^s} + \sigma_{\eta_s}^2}, & \text{(29b)} \end{cases}$$

where $S_r^f$ and $S_r^s$ are the reflected signal power from the target as described in (4) and (6), and $\sigma_{\eta_f}^2$ and $\sigma_{\eta_s}^2$ are the variance of the additive white Gaussian noise (AWGN) in radar.

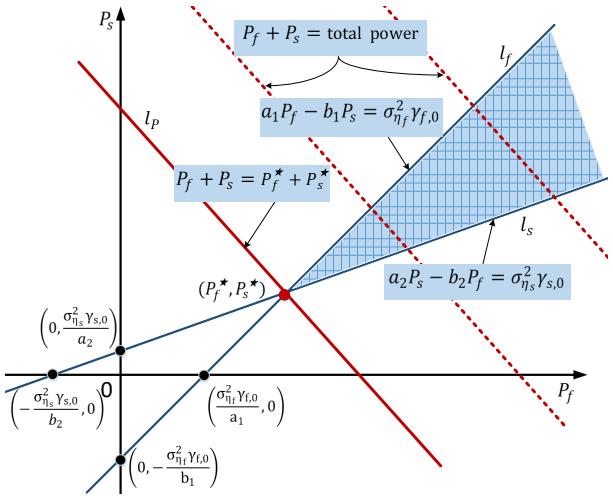


Fig. 4. Illustration of the optimal solution.

Let $\gamma_{f,0}$ and $\gamma_{s,0}$ be the lower threshold of the desired SINR at FR and SR, respectively. Targeting at minimizing the total radar transmission power, we formulate the following optimization problem,

$$\begin{aligned} \min_{\{P_f,P_s\}} \quad & P_f + P_s && \text{(30a)}\\ \text{subject to} \quad & P_f > 0, && \text{(30b)}\\ & P_s > 0, && \text{(30c)}\\ & \overline{\gamma_f} \geq \gamma_{f,0}, && \text{(30d)}\\ & \overline{\gamma_s} \geq \gamma_{s,0}, && \text{(30e)} \end{aligned}$$

The optimization in (30) is a linear programming problem which can be solved by the linear programming (LP) method. As shown in Fig. (4), the optimal solution can be obtained at the intersection of the two lines, where $\overline{\gamma_f} = \gamma_{f,0}$ and $\overline{\gamma_s} = \gamma_{s,0}$.

In order to get the optimal solution, we firstly rewrite (30d) and (30e) with equality as

$$\begin{cases} a_1P_f - b_1P_s = \sigma^2_{\eta_f}\gamma_{f,0}, & \text{(31a)}\\ a_2P_s - b_2P_f = \sigma^2_{\eta_s}\gamma_{s,0}, & \text{(31b)} \end{cases}$$

where $a_1$, $b_1$, $a_2$ and $b_2$ are given by

$$\begin{cases} a_1 = \varepsilon_1^f\varepsilon_2^f\varepsilon_3^f R_f^{-4} - \dfrac{\sqrt{\pi}}{2L}u_H u_{\sigma_f}\gamma_{f,0}\xi\rho\varepsilon_1^f\varepsilon_3^f,\\ b_1 = \dfrac{\sqrt{\pi}}{2L}u_H u_{\sigma_{f,s}}\gamma_{f,0}\xi\rho\varepsilon_1^s\varepsilon_3^f,\\ a_2 = \varepsilon_1^s\varepsilon_2^s\varepsilon_3^s R_s^{-4} - \dfrac{\sqrt{\pi}}{L}u_H u_{\sigma_s}\gamma_{s,0}\xi\rho\varepsilon_1^s\varepsilon_3^s,\\ b_2 = \dfrac{\sqrt{\pi}}{2L}u_H u_{\sigma_{f,s}}\gamma_{s,0}\xi\rho\varepsilon_1^f\varepsilon_3^s. \end{cases} \quad \text{(32)}$$

Existence of the optimal solution to (30) is under the following conditions

$$\begin{cases} a_1 > 0, & \text{(33a)}\\ a_2 > 0, & \text{(33b)}\\ a_1a_2 - b_1b_2 > 0. & \text{(33c)} \end{cases}$$

In (33), the constraints (33a) and (33b) guarantee the inequalities (30d) and (30e), and the constraint (33c) guarantees that the solution region of LP is non-empty, which means the liner inequalities (30d) and (30e) have the valid intersection, i.e., line (31a) has a larger slope than line (31b).

Therefore, we can obtain the optimal solution for the transmission power as

$$\begin{cases} P_f^\star = \dfrac{\sigma^2_{\eta_f}\gamma_{f,0}a_2 + \sigma^2_{\eta_s}\gamma_{s,0}b_1}{a_1a_2 - b_1b_2},\\ P_s^\star = \dfrac{\sigma^2_{\eta_f}\gamma_{f,0}b_2 + \sigma^2_{\eta_s}\gamma_{s,0}a_1}{a_1a_2 - b_1b_2}. \end{cases} \quad \text{(34)}$$

When there is a total power constraint for each of $P_f$ and $P_s$, the minimum required SINR cannot be achieved simultaneously if either $P_f^\star$ or $P_s^\star$ exceeds the constraint. From (34), we can see that both $P_f^\star$ and $P_s^\star$ decrease with the resource reusing probability $\xi$. Hence we can reduce $\xi$ to reduce $P_f^\star$ and $P_s^\star$.

The minimum total transmission power is thus given by

$$(P_f + P_s)_{\min} = \frac{\sigma^2_{\eta_f}\gamma_{f,0}\,(a_2 + b_2) + \sigma^2_{\eta_s}\gamma_{s,0}\,(a_1 + b_1)}{a_1a_2 - b_1b_2}. \quad \text{(35)}$$

Referring to Fig. 4 and (35), we can see that the minimum transmission power increases with the effective density $\xi\rho$ increasing. When $\xi\rho$ increases, the slope $a_1/b_1$ of line $l_f$ decreases and the slope $b_2/a_2$ of line $l_s$ increases. Consequently, the intersection of the two lines $P_f^\star$ and $P_f^\star$ increases.

### *B. Optimization in Multiple-Lane Scenarios*

In multiple-lane scenarios, considering one FR and two SRs, the optimization problem can be formulated as follows

$$\begin{aligned} \min_{\{P_f,P_s\}} \quad & P_f + P_{s_1} + P_{s_2} && \text{(36a)}\\ \text{subject to} \quad & P_f > 0, && \text{(36b)}\\ & P_{s_1} > 0, && \text{(36c)}\\ & P_{s_2} > 0, && \text{(36d)}\\ & \overline{\gamma_f} \geq \gamma_{f,0}, && \text{(36e)}\\ & \overline{\gamma_{s_1}} \geq \gamma_{s_1,0}, && \text{(36f)}\\ & \overline{\gamma_{s_2}} \geq \gamma_{s_2,0}, && \text{(36g)} \end{aligned}$$

where $P_{s_1}$ and $P_{s_2}$ denote the transmission power of radar SR1 and SR2, respectively, $\overline{\gamma_{s_1}}$ and $\overline{\gamma_{s_2}}$ represent the SINR of SR1 and SR2, respectively, and $\gamma_{s_1,0}$, $\gamma_{s_2,0}$ are the thresholds of the mean SINR.

Similar to the process in two-lane scenarios, we can solve the optimization problem by rewriting the constraints (36e), (36f) and (36g) as

$$\begin{cases} a_{m,1}P_f - b_{m,1}P_{s_1} - c_{m,1}P_{s_2} \geq \sigma^2_{\eta_f}\gamma_{f,0}, & \text{(37a)}\\ a_{m,2}P_{s_1} - b_{m,2}P_f - c_{m,2}P_{s_2} \geq \sigma^2_{\eta_{s_1}}\gamma_{s_1,0}, & \text{(37b)}\\ a_{m,3}P_{s_2} - b_{m,3}P_f - c_{m,3}P_{s_1} \geq \sigma^2_{\eta_{s_2}}\gamma_{s_2,0}, & \text{(37c)} \end{cases}$$

where the factors are

$$\begin{cases} a_{m,1} = \varepsilon_1^f \varepsilon_2^f \varepsilon_3^f R_f^{-4} - \dfrac{\sqrt{\pi}}{2L} \displaystyle\sum_{j=1}^{n} \dfrac{\xi_j \rho_j}{m-i+j} u_H u_{\sigma_f} \gamma_{f,0} \varepsilon_1^f \varepsilon_3^f, \\ b_{m,1} = \dfrac{\sqrt{\pi}}{2L} \left[ \displaystyle\sum_{j=1}^{n} \dfrac{\xi_j \rho_j}{m-i+j} + \sum_{k=1}^{i-1} \dfrac{\xi_k \rho_k}{i-k} \right] u_H u_{\sigma_{f,s}} \gamma_{f,0} \varepsilon_1^s \varepsilon_3^f, \\ c_{m,1} = \dfrac{\sqrt{\pi}}{2L} \displaystyle\sum_{k=i+1}^{m} \dfrac{\xi_k \rho_k}{k-i} u_H u_{\sigma_{f,s}} \gamma_{f,0} \varepsilon_1^s \varepsilon_3^f, \\ a_{m,2} = \varepsilon_1^s \varepsilon_2^s \varepsilon_3^s R_{s_1}^{-4} - \dfrac{\sqrt{\pi}}{L} \displaystyle\sum_{j=1}^{n} \dfrac{\xi_j \rho_j}{m-i+j} u_H u_{\sigma_s} \gamma_{s_1,0} \varepsilon_1^s \varepsilon_3^s, \\ b_{m,2} = \dfrac{\sqrt{\pi}}{2L} \left[ \displaystyle\sum_{j=1}^{n} \dfrac{\xi_j \rho_j}{m-i+j} + \sum_{k=i+1}^{m} \dfrac{\xi_k \rho_k}{k-i} \right] \\ \qquad u_H u_{\sigma_{f,s}} \gamma_{s_1,0} \varepsilon_1^f \varepsilon_3^s, \\ c_{m,2} = \dfrac{\sqrt{\pi}}{L} \displaystyle\sum_{k=i+1}^{m} \dfrac{\xi_k \rho_k}{k-i} u_H u_{\sigma_s} \gamma_{s_1,0} \varepsilon_1^s \varepsilon_3^s, \\ a_{m,3} = \varepsilon_1^s \varepsilon_2^s \varepsilon_3^s R_{s_2}^{-4}, \\ b_{m,3} = \dfrac{\sqrt{\pi}}{2L} \displaystyle\sum_{k=i}^{i-1} \dfrac{\xi_k \rho_k}{i-k} u_H u_{\sigma_f} \gamma_{s_2,0} \varepsilon_1^f \varepsilon_3^s, \\ c_{m,3} = \displaystyle\sum_{k=1}^{i-1} \sqrt{\pi} \dfrac{\xi_k \rho_k}{(i-k)L} u_H u_{\sigma_s} \gamma_{s_2,0} \varepsilon_1^s \varepsilon_3^s. \end{cases} \tag{38}$$

Let $P_f + P_{s_1} + P_{s_2} = P_t$. Substituting $P_{s_2} = P_t - P_f - P_{s_1}$ into (37), we obtain

$$\begin{cases} \left(a_{m,1} + c_{m,1}\right) P_f - \left(b_{m,1} - c_{m,1}\right) P_{s_1} \geq \\ \qquad \sigma_{\eta_f}^2 \gamma_{f,0} + c_{m,1} P_t, & \text{(39a)} \\ \left(a_{m,2} + c_{m,2}\right) P_{s_1} - \left(b_{m,2} - c_{m,2}\right) P_f \geq \\ \qquad \sigma_{\eta_{s1}}^2 \gamma_{s_1,0} + c_{m,2} P_t, & \text{(39b)} \\ \left(a_{m,3} + b_{m,3}\right) P_f + \left(a_{m,3} + c_{m,3}\right) P_{s_1} \leq \\ \qquad a_{m,3} P_t - \sigma_{\eta_{s_2}}^2 \gamma_{s_2,0}. & \text{(39c)} \end{cases}$$

In order to ensure that the inequality (39) has a solution, the intersection $(P_f^\star, P_{s_1}^\star)$ of line (39a) and (39b) must meet the condition $\left(a_3^M + b_3^M\right) P_f^\star + \left(a_3^M + c_3^M\right) P_{s_1}^\star \leq a_3^M P_t - \sigma_\eta^2 \gamma_{s_2,0}$. Therefore, we get the inequality for the total transmission power $P_t$ as

$$P_t \geq \frac{\left(a_{m,3} + b_{m,3}\right) P_f^\star + \left(a_{m,3} + c_{m,3}\right) P_{s_1}^\star + \sigma_{\eta_{s2}}^2 \gamma_{s_2,0}}{a_{m,3}}, \tag{40}$$

The optimal solution to (36) is then obtained when the equality is taken in (40), and is given by

$$(P_t)_{min} = \frac{\sigma_{\eta_f}^2 \gamma_{f,0} A_m + \sigma_{\eta_{s_1}}^2 \gamma_{s_1,0} B_m + \sigma_{\eta_{s_2}}^2 \gamma_{s_2,0} C_m}{D_m}. \tag{41}$$

TABLE I
SYMBOLS AND THEIR VALUES USED IN THE PAPER AND SIMULATION.

| Symbol | Numerical Value | Definition/Explanation |
|---|---|---|
| $R^f$ | Variable [m] | Distance from FR to target |
| $R^s$ | Variable [m] | Distance from SR to target |
| $L$ | 6 [m] | Lane spacing |
| $P_r^f$ | Refer to (4) [mW] | Reflected signal of FR |
| $P_r^s$ | Refer to (6) [mW] | Reflected signal of SR |
| $\rho$ | Variable [cars/m] | Vehicles linear density |
| $f_f$ | 76.5 GHz [28] | Central frequency of FR |
| $f_s$ | 77.5 GHz [28] | Central frequency of SR |
| $\xi$ | Variable | Spectrum reusing probability |
| $\gamma_{f,0}$ | 10 [dB] [29] | The $\gamma$ threshold of FR |
| $\gamma_{s,0}$ | 10 [dB] [29] | The $\gamma$ threshold of SR |
| $G_f$ | as given in the paper | Maximum antenna gain of FR |
| $G_s$ | as given in the paper | Maximum antenna gain of SR |
| $\sigma_c$ | 30dBsm [29] | Front-Radar cross-section |
| $\sigma_c^s$ | 30dBsm [29] | Side-Radar cross-section |
| $g^f(\beta)$ | Refer to (14) | Gain in different direction (FR) |
| $g^s(\beta)$ | Refer to (14) | Gain in different direction (SR) |
| $\mathbf{H}_i$ | - | Interfering signals fading progresses |
| $u_H$ | 1 | the mean value of $\mathbf{H}_i$ |
| $c$ | 3e8[m/s] | Speed of light |
| $\varepsilon_1^f/\varepsilon_1^s$ | Refer to (5) and (7) | Radar-specific transmission constant |
| $\varepsilon_2^f/\varepsilon_2^s$ | Refer to (5) and (7) | Target-specific constant |
| $\varepsilon_3^f/\varepsilon_3^s$ | Refer to (5) and (7) | Radar-specific received constant |

Where

$$\begin{cases} A_m = c_{m,2}c_{m,3} - a_{m,2}a_{m,3} - a_{m,3}b_{m,2} - b_{m,3}c_{m,2} \\ \qquad - a_{m,2}b_{m,3} - b_{m,2}b_{m,3}, \\ B_m = b_{m,3}c_{m,1} - a_{m,1}a_{m,3} - a_{m,3}b_{m,1} - c_{m,1}c_{m,3} \\ \qquad - a_{m,1}c_{m,3} - b_{m,1}b_{m,3}, \\ C_m = b_{m,1}b_{m,1} - a_{m,1}a_{m,1} - a_{m,1}c_{m,1} - b_{m,1}c_{m,1} \\ \qquad - a_{m,1}c_{m,1} - b_{m,1}c_{m,1}, \\ D_m = a_{m,3}b_{m,1}b_{m,1} - a_{m,1}a_{m,1}a_{m,3} + a_{m,1}b_{m,3}c_{m,1} \\ \qquad + a_{m,1}c_{m,1}c_{m,3} + b_{m,1}b_{m,3}c_{m,1} + b_{m,1}c_{m,1}c_{m,3}. \end{cases} \tag{42}$$

We can see that the optimal power is obtained at the intersection of the three lines.

## VI. Simulation Results

In this section, we present simulation results to verify the accuracy of the derived analytical expressions on radar interference, and test the optimality of our proposed power minimization scheme. Important observations are highlighted in Italic in this section.

Referring to the simulation parameters in Table I, our system setup is described as follows. We generate the number and locations of vehicles randomly following the PPP with the vehicle density paramater $\rho$, and allocate vehicles using the same frequency with the typical vehicle according to the frequency reuse probability $\xi$. The pathloss and channel fading of the effective signal and interference signals are simulated following the description in Section II.B. Most of radar parameters are similar to those used in [7], [28], [29], except for the radiation patterns of the antennas.

The directional radiation patterns of the radar antennas used in this paper are generated as follows. Let $\theta_f$ and $\theta_s$ be the 3dB beamwidth of the main-lobe of FR and SR, respectively.

From Eq. (14), we can obtain $\sigma_f^2$ and $\sigma_s^2$ corresponding to the 3dB beamwidth as

$$\begin{cases} \sigma_f^2 = -\dfrac{\theta_f^2}{8\ln g^f(\theta_f/2)} = \dfrac{\theta_f^2}{8\ln 2} \\ \sigma_s^2 = -\dfrac{\theta_s^2}{8\ln g^s(\theta_f/2)} = \dfrac{\theta_s^2}{8\ln 2}. \end{cases} \tag{43}$$

Generally, SR has wider beamwidth than FR. According to [29], the beamwidth of automotive radars is typically between $15^\circ$ to $80^\circ$.

Since the maximum antenna gain is typically linked to the beamwidth and radiation pattern, we set $G_f = 1/(\sqrt{2\pi}\sigma_f)$ and $G_s = 1/(\sqrt{2\pi}\sigma_s)$, being the antenna gains via the Gaussian waveform for FR and SR, respectively. Note that since we only consider the gain at the horizontal plane, it is much smaller than the actual total antenna gain. Hence the values of the interference power and transmission power minimization results presented in this section are only relative, and we focus on investigating their relationship with the system parameters and verifying the accuracy of the analytical results.

### A. Radar Mean Interference

In this part, we focus on studying how the interference, as well as the signal-to-interference power ratio (SIR), is affected by different system parameters in a two-lane scenario. Without considering noise, the mean SIR is defined as $\text{SIR}(\overline{I^f}) = S_r^f/\overline{I^f}$ and $\text{SIR}(\overline{I^s}) = S_r^s/\overline{I^s}$ for FR and SR, respectively. The transmission power is set as $P_f = P_s = 10$ mW.

The mean interference power at FR and SR with varying vehicle density $\rho$ of the PPP geometrical model is shown in Fig. 5. We set $\theta_f = 15^\circ$ and $\theta_s = 80^\circ$, i.e., $\sigma_f = 0.1112$ and $\sigma_s = 0.5929$ for FR and SR, respectively. The simulated interference power is shown to be linearly proportional to vehicle density, and matches very well with the analytical one. We also compare our results with those in [7] which assumes the use of a directional antenna with the same antenna gain over a range of directions. The mean interference for [7] is shown to be much larger than ours, which indicates that the use of directional antenna can significantly reduce the interference.

To evaluate the accuracy of approximating the directional radiation pattern of a radar by a Gaussian function, we consider a uniform linear antenna array (ULA) here. Fig. 7 presents the radiation pattern for the ULAs and their Gaussian approximations for FR and SR. The beamwidth of the ULA is determined by the number of antennas in the array, where antennas are spaced at half wavelength. We introduce a metric, *mean normalized approximation error (MNAE)* $\overline{\delta}$, to evaluate the approximation accuracy for the interference. The MNAE is defined as

$$\overline{\delta} = \frac{1}{K}\left[\sum_{i=1}^{K} \frac{|\overline{I_i^{Gau}} - \overline{I_i^{ULA}}|}{\overline{I_i^{Gau}}}\right] \times 100\%, \tag{44}$$

where $\overline{I_i^{Gau}}$ and $\overline{I_i^{ULA}}$ denote the mean interference obtained in the $i$-th test for the Gaussian approximation and the actual ULA, respectively, $K$ is the number of tests. Fig. 6 plots

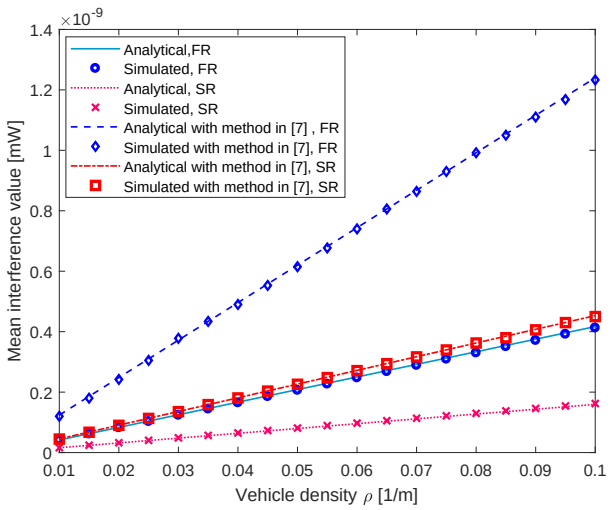


Fig. 5. Analytical and simulated mean interference power at SR and FR, where $\sigma_f = 0.1112, \theta_f = 15^\circ$, and $\sigma_s = 0.5929, \theta_s = 80^\circ$; $\xi = 4\%$.

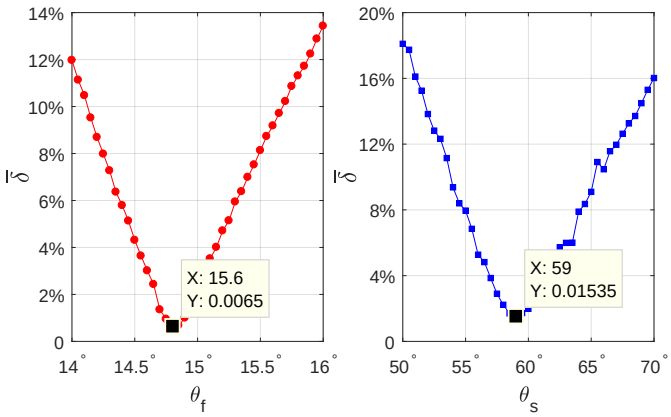


Fig. 6. MNAE between ULA and its Gaussian approximation for FR (left subfigure) and SR (right subfigure), with various beamwidth values.

the MNAE for FR and SR with different parameters of the Gaussian approximation to the two ULA beams shown in Fig. 7. We obtain the minimum MNAE $0.65\%$ when $\theta_f = 15.6^\circ$ for FR, and $1.54\%$ when $\theta_s = 59^\circ$ for SR. The waveforms for the specific Gaussian approximations with these parameters are plotted in Fig. 7. The MNAE is very small, which means that the Gaussian function is an accurate approximation to the radiation pattern of real antenna arrays.

In Fig. 8, we show more details of the composition of interference. It is interesting to see that *most of the interference to one radar is from the same type of other radars*. As can be seen from Fig. 8 (a), more than $75\%$ of the interference to FR is from other FRs, and the narrower the beamwidth is, the higher the proportion is. Similarly, from Fig. 8 (b), we can see that more than $74\%$ of the interference is from SR-to-SR for the simulated beamwidth ranging from 40 to 80 degrees. This suggests that the cross-impact between FR and SR shall be considered differently to their respective self-impact when using resource allocation such as frequency allocation for interference mitigation.

We further study the impact of beamwidth on interference

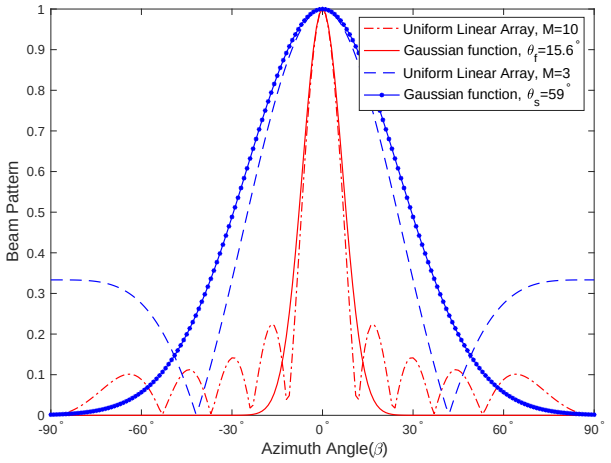


Fig. 7. Radiation pattern of a ULA and its Gaussian approximation for FR, where $\sigma_f = 0.1156, \theta_f = 15.6°$ and SR, where $\sigma_s = 0.4373, \theta_s = 59°$. In this specific example, the ULA has 10 and 3 antennas for the FR and SR, respectively.

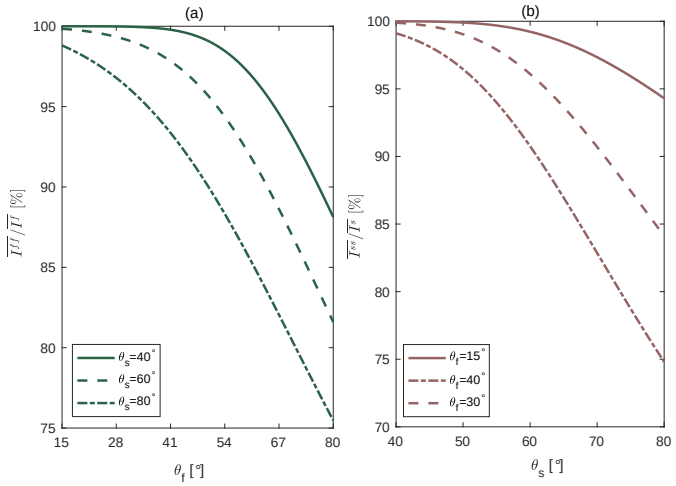


Fig. 8. Ratio $\overline{I^{ff}}/\overline{I^f}$ of FR (left sub-figure) and $\overline{I^{ss}}/\overline{I^s}$ of SR (right sub-figure), $\rho = 1/50$.

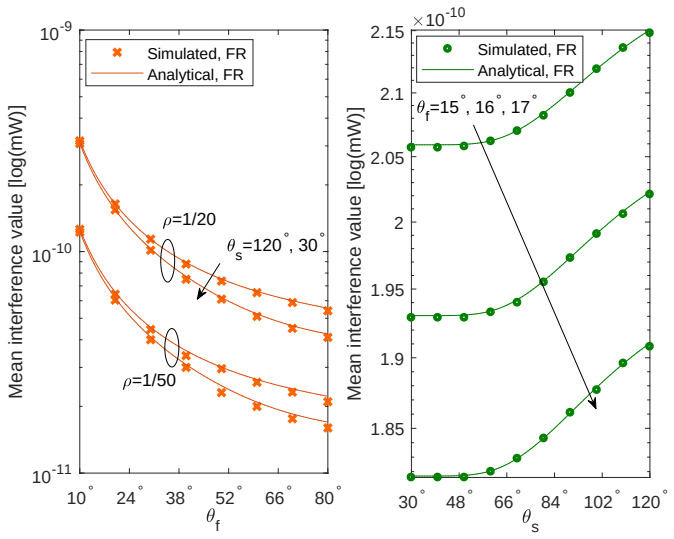


Fig. 9. Analytical and simulated results for the mean interference power at FR with varying beamwidth. In the right sub-figure, $\rho = 1/20$; $\xi = 4\%$.

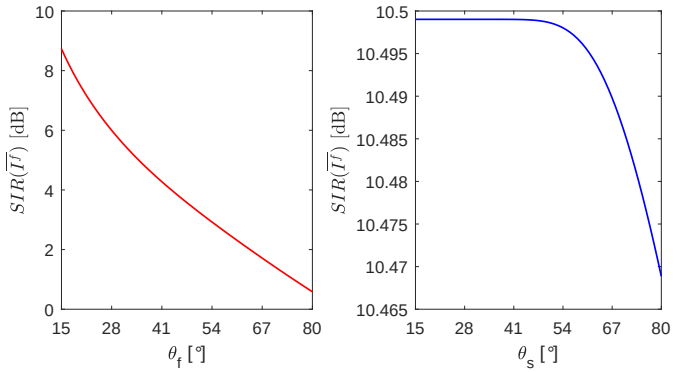


Fig. 10. Variation of the SIR for FR with beamwidth, where $R_f = 30$m, $\theta_s = 60°$ (left) and $\theta_f = 10°$ (right), $\rho = 1/50$; $\xi = 4\%$.

and present the results in Fig. 9. We can see that the mean interference power $\overline{I^f}$ decreases rapidly with $\theta_f$ increasing but increases slightly with $\theta_s$ increasing from 30° to 120°. This is consistent with the results in Fig. 8 (a). In Fig. 10, we demonstrate how the mean SIR for FR is affected by beamwidth. As shown in Fig. 10, SIR($\overline{I^f}$) decreases with either the beamwidth $\theta_f$ or $\theta_s$ increasing. The change of SIR($\overline{I^f}$) is very small with varying $\theta_s$, as $\overline{I^f}$ varies slowly with $\theta_s$. Combined with the results in Fig. 9, we see that although the mean interference power at FR decreases, the mean SIR is reduced with $\theta_f$ increasing. This indicates that the signal power decreases faster than the interference. Therefore, *FR with a narrower beamwidth $\theta_f$ can achieve better overall sensing performance.*

We also present similar results for SR in Fig. 11. We can obtain similar observations to those for FR, and can conclude that using a SR with narrower beamwidth can generate overall better performance for side sensing. We can also see that *the mean interference power at SR is comparable to that at FR, even though it has a much wider beamwidth.*

Note that the above observations for FR and SR are based on the assumption that the received effective echo signal is mainly from the main beam direction. When the sensing direction deviates significantly from the centre, the conclusions may need to be further revisited.

### B. Power Minimization Results

For power minimization, we need to set the noise power in the radar receiver. Since our antenna gain is relative, we cannot directly set up the receiver noise floor according to, e.g., the thermal noise and device bandwidth. Instead, we determine a noise floor relative to the antenna gain, to make the simulation results close to practical realizations. This is achieved by setting a desired received SNR for targeted sensing distances. As an example, we consider the sensing distances $R_f = 25$m and $R_s = 15$m, the transmission power 10 mW, and the desired received SNR 15 dB. For radar beamwidth $\theta_f = 15°$ and $\theta_s = 60°$, without considering interference, we can work out the equivalent variance of AWGN for FR and SR as

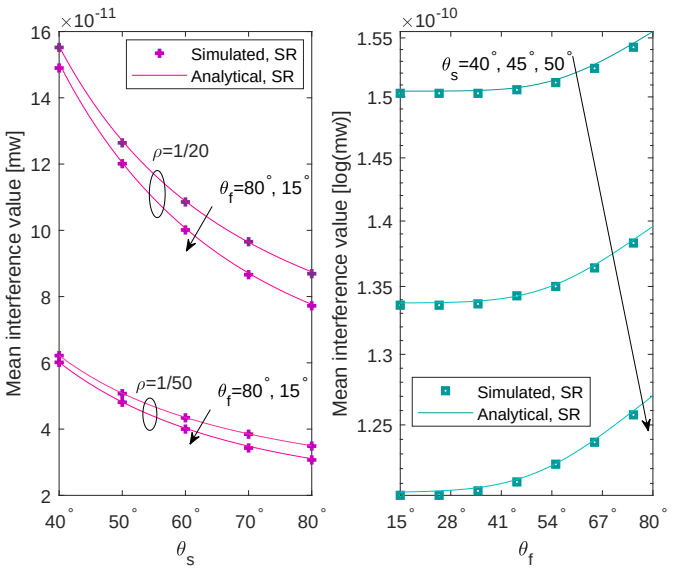


Fig. 11. Analytical and simulated results for the mean interference power of SR with varying beamwidth. In the right sub-figure, $\rho = 1/20$; $\xi = 4\%$.

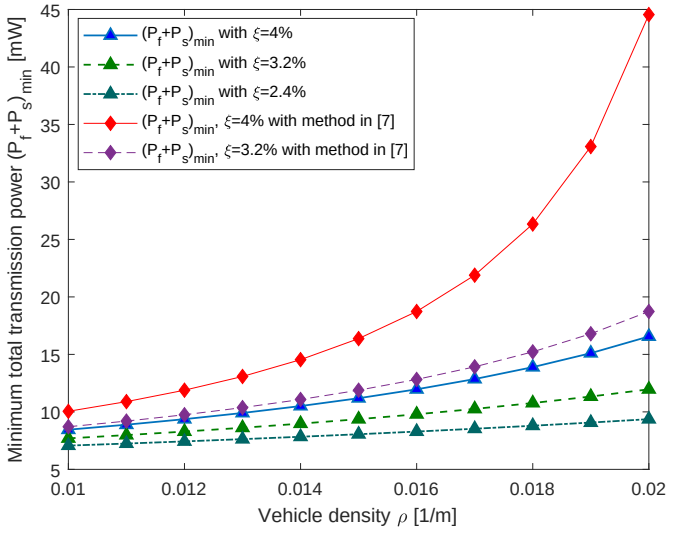


Fig. 12. Total minimized transmission power with a Gaussian beam for varying vehicle densities in a two-lane scenario.

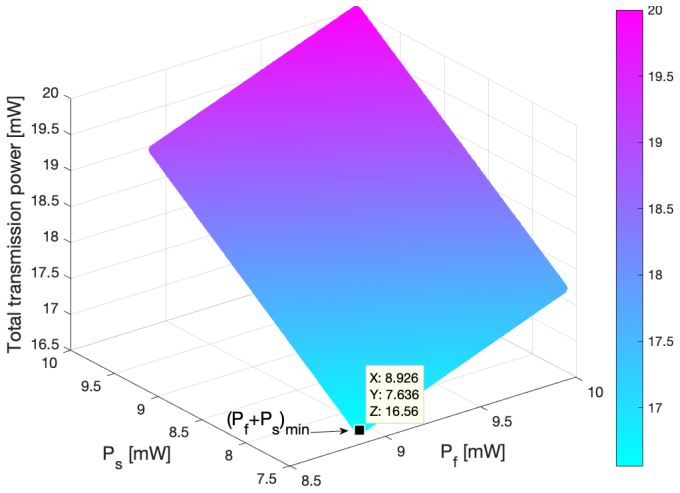


Fig. 13. Optimal total transmission power based on simulated results in two-lane case, where $\theta_f = 15°$, $\theta_s = 60°$, $\xi = 4\%$ and $\rho = 0.02$.

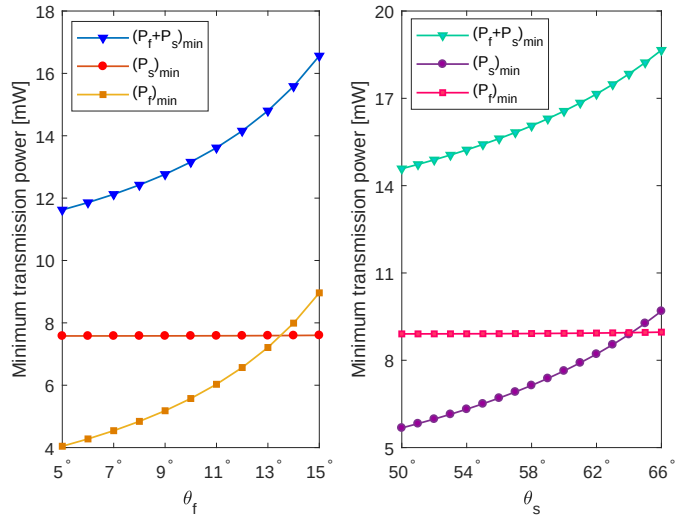


Fig. 14. Minimum transmission power with varying $\theta_f$ and $\theta_s$ in a two-lane scenario, where $\rho = 1/50$ and $\xi = 4\%$, $\theta_s = 60°$ (left), and $\theta_f = 15°$ (right).

$\sigma^2_{\eta_f} = 4.0392 \times 10^{-11}$mW and $\sigma^2_{\eta_s} = 1.5076 \times 10^{-11}$mW, respectively.

We first present results for two-lanes (from Figs. 12 to 14) and then for multi-lanes. For multi-lanes, we set the numbers of lanes $m$ and $n$ as $m = n = 3$ and assume that the typical vehicle locates in the middle lane. Similar parameters are used in two-lane and multi-lane scenarios.

In Fig. 12, we demonstrate how the minimized transmission power is affected by the vehicle density $\rho$. The figure shows that the minimum power $P_f^* + P_s^*$ increases almost linearly with $\rho$ increasing, particularly when $\xi$, the resource reusing probability, is small. As expected, it also increases with $\xi$ increasing, as interference also grows. For comparison, the results for [7] are also presented. Its optimized transmission power is shown to be significantly larger than ours. The comparison shows clearly the great impact of using directional antenna in reducing the required transmission power. In Fig.13, we show the zone of different combinations of the transmission power from FR and SR that can meet the required minimum SINR. We can see that the optimized analytical solution indeed achieves the minimum transmission power.

In Fig. 14, we illustrate the relationship between the minimized transmission power and beamwidth $\theta_f$ and $\theta_s$. In the left sub-figure, when $\theta_s$ is fixed to 60°, both $P_f^* + P_s^*$ and $P_f^*$ increase with $\theta_f$ increasing, and $P_s^*$ almost remains unchanged. This is because the mean interference power of SR only varies insignificantly with $\theta_f$. In the right sub-figure, when $\theta_f$ is fixed to 15°, both $P_f^* + P_s^*$ and $P_s^*$ increase with $\theta_s$ increasing, and $P_f^*$ almost remains unchanged.

In Fig. 15, we show that similar to the two-lane case, the minimum transmission power in a multi-lane scenario increases almost linearly with the vehicle density $\rho$ increasing. Comparing Fig. 15 with 12, we can see the averaged power

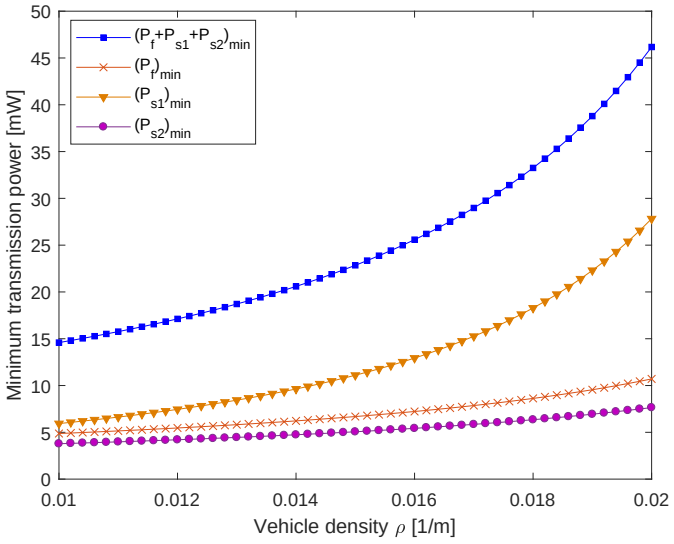


Fig. 15. Variation of minimum transmission power with vehicle density in a multi-lane scenario, where $\xi = 4\%$.

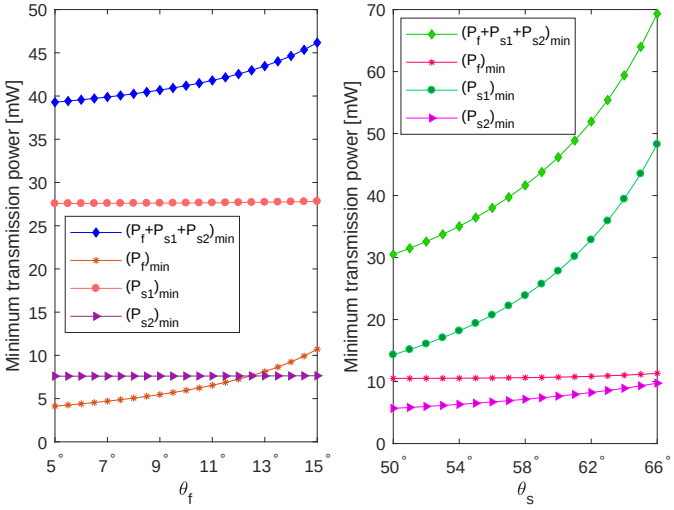


Fig. 16. Minimum transmission power with varying $\theta_f$ and $\theta_s$, where $\theta_s = \theta_{s_1} = \theta_{s_2}$, $\rho = 1/50$ and $\xi = 4\%$. In the left subfigure, $\theta_{s_1} = \theta_{s_2} = 60°$, and in the right sub-figure, $\theta_f = 15°$.

per radar increases in the multi-lane case.

In Fig. 16, we demonstrate how the minimized transmission power changes with varying beamwidth in the three-lane case. In the left sub-figure, we note that the optimized transmission power $(P_{s_1})_{min}$ and $(P_{s_2})_{min}$ remain nearly constant with $\theta_f$ increasing, while $(P_f)_{min}$ increases rapidly with $\theta_f$ increasing. This is because the mean interference power of SR1 and SR2 only changes slightly with the beamwidth $\theta_f$ of FR, as can be seen from Fig.11. We also note that compared to the two-lane case, $(P_{s_2})_{min}$ remains almost unchanged and $(P_f)_{min}$ only slightly increases, benefiting from the narrow beamwidth; however, $(P_{s_1})_{min}$ is much larger than $(P_{s_2})_{min}$ because the SR on the right side of the typical vehicle sees more interference. We can have similar observations for SR from the right subfigure of Fig. 16.

## VII. Conclusions

In this paper, we introduced a stochastic geometry method to model the location and density of vehicles and hence automotive radars. We considered both front- and side-mounted radars with directional antennas, and developed a framework for analytically calculating the mean interference power seen by each radar. Approximating the antenna radiation pattern with a Gaussian function, we derived closed-form expressions for the mean interference power. Based on the interference analysis, we then formulated the cost function for minimizing the total transmission power of radars on each vehicle. With the SINR constraints for each radar, we derived optimal solutions that minimize the total transmission power. Linking the antenna gain to the main parameter in the Gaussian function, we demonstrated how the interference and the SIR vary with the beamwidth of both radars.

Some of the important insights obtained from this study are summarized below:

- The side-mounted radar sees interference comparable to the front-mounted radar, although it has a much larger beamwidth;
- In general, narrower beamwidth leads to larger interference but higher SIR for both radars, and overall, both FR and SR with a narrower beamwidth can achieve better overall sensing performance;
- Interference power is shown to be linearly proportional to vehicle density;
- Most of the interference to one radar is from the same type of other radars, which should be an important factor to be considered by resource allocation;
- The optimized transmission power for different radars changes differently from the two-lane to three-lane cases: the power for SRs facing more lanes is much larger than those facing less lanes, while the power of FR is only slightly increased due to the narrow beamwidth.

Our results provide important guidance for developing ad-hoc automotive radar networks and optimizing their frequency resource access and allocation. Our work in this paper can be extended to provide more accurate characterization for radar interference, by considering actual radar operations, such as partially-overlapped frequency band of chirp waveforms due to asynchronous operation of FMCW radars, and the repetition length and period of chirp waveforms.

## References

[1] J. Hasch, E. Topak, R. Schnabel, T. Zwick, R. Weigel, and C. Waldschmidt, "Millimeter-wave technology for automotive radar sensors in the 77 GHz frequency band," *IEEE Transactions on Microwave Theory and Techniques*, vol. 60, no. 3, pp. 845–860, 2012.

[2] K. Bengler, K. Dietmayer, B. Farber, M. Maurer, C. Stiller, and H. Winner, "Three decades of driver assistance systems: Review and future perspectives," *IEEE Intelligent Transportation Systems Magazine*, vol. 6, no. 4, pp. 6–22, 2014.

[3] M. Goppelt, H.-L. Blöcher, and W. Menzel, "Automotive radar–investigation of mutual interference mechanisms," *Advances in Radio Science*, vol. 8, no. B. 3, pp. 55–60, 2010.

[4] ——, "Analytical investigation of mutual interference between automotive fmcw radar sensors," in *2011 German Microwave Conference*. IEEE, 2011, pp. 1–4.

[5] G. M. Brooker, "Mutual interference of millimeter-wave radar systems," *IEEE Transactions on Electromagnetic Compatibility*, vol. 49, no. 1, pp. 170–181, 2007.

[6] T. Schipper, S. Prophet, M. Harter, L. Zwirello, and T. Zwick, "Simulative prediction of the interference potential between radars in common road scenarios," *IEEE Transactions on Electromagnetic Compatibility*, vol. 57, no. 3, pp. 322–328, 2015.

[7] A. Al-Hourani, R. J. Evans, S. Kandeepan, B. Moran, and H. Eltom, "Stochastic geometry methods for modeling automotive radar interference," *IEEE Transactions on Intelligent Transportation Systems*, vol. 19, no. 2, pp. 333–344, 2018.

[8] C. Shi, F. Wang, M. Sellathurai, and J. Zhou, "Non-cooperative game theoretic power allocation strategy for distributed multiple-radar architecture in a spectrum sharing environment," *IEEE Access*, vol. 6, pp. 17 787–17 800, 2018.

[9] A. Deligiannis, S. Lambotharan, and J. A. Chambers, "Game theoretic analysis for MIMO radars with multiple targets," *IEEE transactions on aerospace and electronic systems*, vol. 52, no. 6, pp. 2760–2774, 2016.

[10] Z. Geng, H. Deng, and B. Himed, "Adaptive radar beamforming for interference mitigation in radar-wireless spectrum sharing," *IEEE Signal Processing Letters*, vol. 22, no. 4, pp. 484–488, 2014.

[11] T.-N. Luo, C.-H. E. Wu, and Y.-J. E. Chen, "A 77-GHz CMOS automotive radar transceiver with anti-interference function," *IEEE Transactions on Circuits and Systems I: Regular Papers*, vol. 60, no. 12, pp. 3247–3255, 2013.

[12] H. Godrich, A. P. Petropulu, and H. V. Poor, "Power allocation strategies for target localization in distributed multiple-radar architectures," *IEEE Transactions on Signal Processing*, vol. 59, no. 7, pp. 3226–3240, 2011.

[13] C. Shi, F. Wang, M. Sellathurai, J. Zhou, and S. Salous, "Power minimization-based robust OFDM radar waveform design for radar and communication systems in coexistence," *IEEE Transactions on Signal Processing*, vol. 66, no. 5, pp. 1316–1330, 2017.

[14] C. Shi, F. Wang, S. Salous, and J. Zhou, "Joint subcarrier assignment and power allocation strategy for integrated radar and communications system based on power minimization," *IEEE Sensors Journal*, 2019.

[15] C. Shi, F. Wang, M. Sellathurai, J. Zhou, and S. Salous, "Low probability of intercept-based optimal power allocation scheme for an integrated multistatic radar and communication system," *IEEE Systems Journal*, 2019.

[16] Y. Zhou, H. Zhou, F. Zhou, Y. Wu, and V. C. Leung, "Resource allocation for a wireless powered integrated radar and communication system," *IEEE Wireless Communications Letters*, vol. 8, no. 1, pp. 253–256, 2018.

[17] M. K. Saleem, H. Vettikaladi, M. A. Alkanhal, and M. Himdi, "Lens antenna for wide angle beam scanning at 79 GHz for automotive short range radar applications," *IEEE Transactions on Antennas and Propagation*, vol. 65, no. 4, pp. 2041–2046, 2017.

[18] M. J. Farooq, H. ElSawy, and M.-S. Alouini, "A stochastic geometry model for multi-hop highway vehicular communication," *IEEE Transactions on Wireless Communications*, vol. 15, no. 3, pp. 2276–2291, 2015.

[19] Z. Tong, H. Lu, M. Haenggi, and C. Poellabauer, "A stochastic geometry approach to the modeling of DSRC for vehicular safety communication," *IEEE Transactions on Intelligent Transportation Systems*, vol. 17, no. 5, pp. 1448–1458, 2016.

[20] H. ElSawy, A. Sultan-Salem, M.-S. Alouini, and M. Z. Win, "Modeling and analysis of cellular networks using stochastic geometry: A tutorial," *IEEE Communications Surveys & Tutorials*, vol. 19, no. 1, pp. 167–203, 2016.

[21] J. Zhang and J. G. Andrews, "Distributed antenna systems with randomness," *IEEE Transactions on Wireless Communications*, vol. 7, no. 9, pp. 3636–3646, 2008.

[22] S. P. Weber, X. Yang, J. G. Andrews, and G. De Veciana, "Transmission capacity of wireless ad hoc networks with outage constraints," *IEEE Transactions on Information Theory*, vol. 51, no. 12, pp. 4091–4102, 2005.

[23] B. Blaszczyszyn, P. Mühlethaler, and Y. Toor, "Maximizing throughput of linear vehicular ad-hoc networks (VANETs)—a stochastic approach," in *2009 European Wireless Conference*. IEEE, 2009, pp. 32–36.

[24] M. Haenggi, J. G. Andrews, F. Baccelli, O. Dousse, and M. Franceschetti, "Stochastic geometry and random graphs for the analysis and design of wireless networks," *IEEE Journal on Selected Areas in Communications*, vol. 27, no. 7, pp. 1029–1046, 2009.

[25] M. Haenggi, "Mean interference in hard-core wireless networks," *IEEE Communications Letters*, vol. 15, no. 8, pp. 792–794, 2011.

[26] M. I. Skolnik, "Introduction to radar," *Radar handbook*, vol. 2, p. 21, 1962.

[27] M. Haenggi, *Stochastic geometry for wireless networks*. Cambridge University Press, 2012.

[28] International Telecommunications Union (ITU), document ITU-R M.2057-0., "Systems characteristics of automotive radars operating in the frequency band 76-81 GHz for intelligent transport systems applications," 2014. [Online]. Available: https://www.itu.int/rec/R-REC-M.2057-0-201402-S/en

[29] J. Hasch, E. Topak, R. Schnabel, T. Zwick, R. Weigel, and C. Waldschmidt, "Millimeter-wave technology for automotive radar sensors in the 77 GHz frequency band," *IEEE Transactions on Microwave Theory and Techniques*, vol. 60, no. 3, pp. 845–860, 2012.